RSC Advances

ROYAL SOCIETY OF CHEMISTRY

www.rsc.org/advances

Graphical Abstract

A water soluble non-fluorescent structurally characterised distorted square planar copper(II) complex (**1**) selectively senses HSO_4^- ions as low as 3.18×10^{-7} M in water : DMSO (9 : 1, v/v) HEPES buffer at biological pH, which has been established by thorough experimental and theoretical studies. This biofriendly probe is also useful for the distribution of intracellular HSO_4^- ions under a fluorescence microscope.

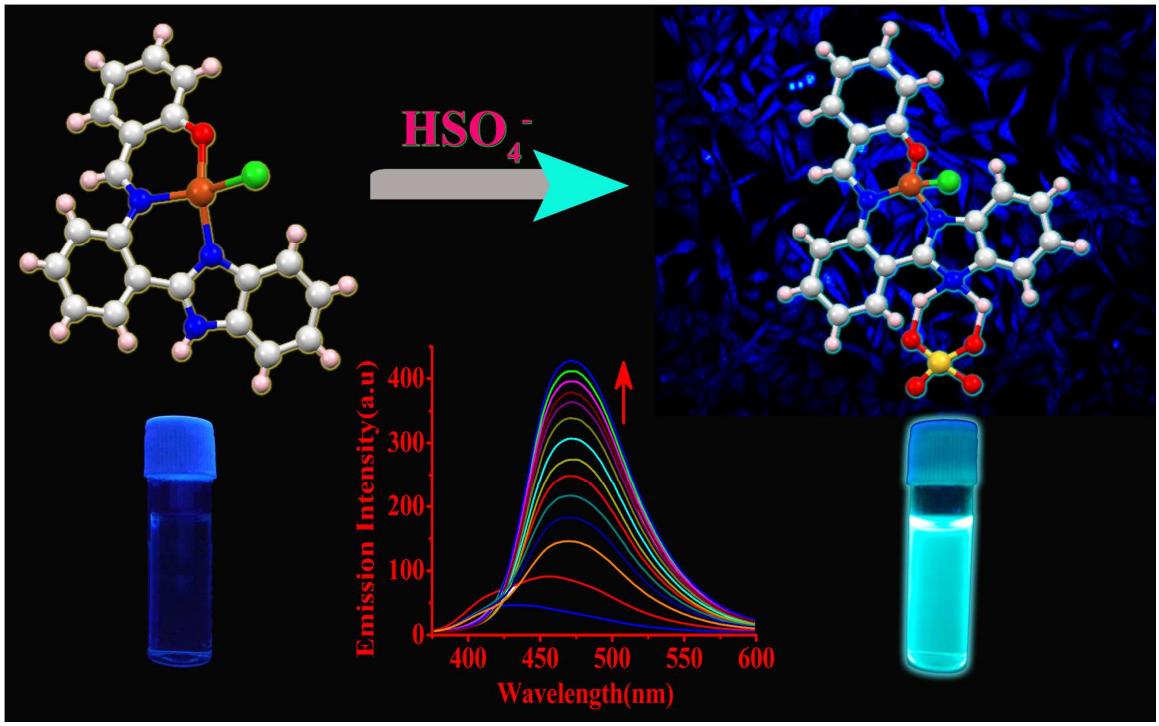

Journal Name

RSC Publishing

ARTICLE

A water soluble copper(II) complex as a HSO_4^- ion selective turn-on fluorescent sensor applicable in living cell imaging†

Buddhadeb Sen, Manjira Mukherjee, Siddhartha Pal, Supriti Sen and Pabitra Chattopadhyay*

Cite this: DOI: 10.1039/x0xx00000x

Received 00th January 2014,
Accepted 00th January 2014

DOI: 10.1039/x0xx00000x

www.rsc.org/

A water soluble non-fluorescent copper(II) complex (**1**) of a quinazoline derivative formulated as [Cu(L′)(Cl)] (**1**) has been synthesized in a facile synthetic method and characterized by physico-chemical and spectroscopic tools along with the single crystal X-ray crystallography for detailed structural analysis. **1** behaves as a highly selective and sensitive for HSO_4^- ions through the enhancement of fluorescence of the system based on intermolecular hydrogen bonding assisted chelation enhanced fluorescence (CHEF) process in '*turn-on*' style, which has been confirmed by systematic optical techniques and electrochemical studies. This mode of sensing pathway and binding of HSO_4^- ions with the receptor **1** has also been validated by optimizing the structures of [Cu(L′)(Cl)] (**1**) and [Cu(L′)(Cl)].HSO_4^- adduct (**2**) with the help of theoretical calculations. This non-cytotoxic probe senses HSO_4^- ions as low as 3.18×10^{-7} M in water : DMSO (9 : 1, v/v) at biological pH (using 1 mM HEPES buffer) and it is also useful for the detection of intracellular HSO_4^- ions under a fluorescence microscope.

Introduction

Anions play a crucial role in a wide range of agricultural, biological systems, environmental and industrial processes.[1] Hence, the design and development of selective optical chemosensors for various anions have gained considerable attention.[2] Sulfate and hydrogen sulfate are among the most important macronutrients in cells and is the fourth most abundant anion in human plasma (300 mM). They are required for proper cell growth and development of the organism. They are involved in a variety of important biological processes, including biosynthesis and detoxification *via* sulfation of many endogenous and exogenous compounds.[3] They also play appreciable role in radioactive waste remediation.[4] Amphiphilic hydrogen sulfate tends to dissociate at high pH to yield sulfate ions. Despite their importance in cellular activities, high levels of sulfate in rain water, surface water and ground water correlated with emissions of sulfur dioxide from anthropogenic sources decreases the pH level of soil and water. Health concerns regarding contamination of sulfate in drinking water have been raised because of reports of diarrhea and it also causes irritation of skin and eyes and even respiratory paralysis.[5] Hydrogen sulfate anion has a large standard Gibbs energy of hydration (-1080 kJ mol^{-1}), the recognition and separation of the hydrogen sulfate anion from an aqueous media is a challenging task.[6]

However, there are several fluorogenic chemosensors for HSO_4^- ions have been reported[7] and most of them are lack of selectivity, low water solubility, and laborious multistep synthetic procedures, not practicable for intracellular imaging. But in all cases, organic moieties have been reported as chemosensor and report of non-fluorescent coordination complex as HSO_4^- ion selective chemosensor is not on hand in literature. Therefore, it is a challenging to the coordination chemists to obtain a water soluble cell permeable coordination complex as HSO_4^- ion selective chemosensor with high sensitivity and low detection limit.

Keeping all the above facts in mind, we have synthesised a water soluble copper(II) complex of quinazoline based ligand (HL), to act as a cell permeable HSO_4^- ion selective sensor in aqueous solvent. Here, both HL and the complex [Cu(L′)(Cl)] (**1**) have been structurally characterized by single crystal X-ray crystallography. Complex **1** behaves as a highly selective and sensitive fluorescent probe for HSO_4^- ions in water : DMSO (9 : 1, v/v) at biological pH (using 1 mM HEPES buffer) at 25 °C upto a very low concentration (3.18×10^{-7} M) of HSO_4^- ions through intermolecular hydrogen bonding assisted chelation enhanced fluorescence (CHEF) process. The probe (complex **1**) was also useful to detect the presence of bisulphate ions by acquiring image of HeLa cells under a fluorescence microscope. To the best of our knowledge so far, the paramagnetic water soluble copper(II) complex as a cell permeable HSO_4^- ion selective 'turn on' fluorescence probe is still unexplored.

Experimental section

Synthesis of 2-(5,6-dihydro-benzo[4,5]imidazo[1,2-c]quinazolin-6-yl)-phenol (HL)

HL was prepared following a reported procedure by refluxing *2-(2-aminophenyl)benzimidazole*, (2.09 g, 10.0 mmol) with *2-hydroxy-benzaldehyde* (1.22 g, 10.0 mmol) in methanol (Scheme S1 ESI†).[8] Pale yellow colored rectangular shaped single crystals of (HL) suitable for X-ray crystallography were obtained on slow evaporation of the DMF-methanol mixture.

HL. $C_{20}H_{15}N_3O$: Anal. Found: C, 76.89; H, 4.95; N, 13.17; Calc. C, 76.66; H, 4.82; N, 13.41. ESI-MS: $[M + H]^+$, m/z, 314.3490 (100 %) (Fig. S1 ESI†) (calcd.: m/z, 314.12; where M = molecular weight of HL]; ^{1}H NMR (δ, ppm in DMSO-d_6): 10.26 (s, 1H, O-H) 7.96 (dd, 1H); 7.65 (d, 1H); 7.31-7.23 (m, 4H); 7.20-7.11 (m, 2H); 6.87-6.73 (m, 3H); 6.60 (dd, 1H); 6.44 (dd, 1H); 4.40 (s, 1H, N-H) (Fig. S2 ESI†). Yield: 90%.

Synthesis of [Cu(L′)(Cl)] (1) and 1-HSO_4^- assembly (2)

The preparation of [Cu(L′)(Cl)] complex **(1)** and **1**-HSO_4^- assembly was carried out *viz*. Scheme 1.

[Cu(L′)(*Cl*)]. A solution of copper(II) chloride dehydrate (0.5 mmol, 86 mg) in methanol was added drop wise into the solution of HL (0.5 mmol, 157 mg) in MeOH-DMF at stirring condition. The mixture was stirred for another 8.0 h and then the resulting solution was kept aside at ambient temperature. After a few days, green colored rod shaped crystals were collected by filtration followed by washing with cold water and methanol.

[Cu(L′)(*Cl*)]. $C_{20}H_{14}N_3OCuCl$: Anal. Found: C, 58.19; H, 3.32; N, 10.57; Cu, 15.19; Calc. C, 58.40; H, 3.43; N, 10.22; Cu, 15.45. ESI-MS: $[M+Na]^+$, m/z, 433.2409 (obsd. with 9 % abundance) (calcd.: m/z, 433.02) (Fig. S3 ESI†).

Na[Cu(L′)(Cl)].HSO_4. The preparation of the solid compound of hydrogen sulphate was carried out by mixing 2 ml MeOH solution of $NaHSO_4$ (one drop of water is added just to moist) (30 mg, 0.25 mmol) slowly to the stirred 8 mL MeOH solution of [Cu(L′)(Cl)] (102.8 mg, 0.25 mmol) and stirred for 5.0 h. Green colored reaction mixture was filtered and kept for slow evaporation. After a few days, green colored mass was obtained by filtration followed by washing with cold methanol and then dried in *vacuo* for performing the characterization.

Na[Cu(L′)(Cl)].HSO_4. $NaC_{20}H_{15}N_3O_5SCuCl$: Anal. Found: C, 45.01; H, 2.91; N, 8.11; S, 5.91; Cu, 11.77. Calc. C, 45.20; H, 2.85; N, 7.91; S, 6.03; Cu, 11.96. IR (KBr, cm^{-1}): $\nu_{C=N}$, 1608.63, $\nu_{S=O}$ 1184.29 (Fig. S4 ESI†). ESI-MS: $[M+H]^+$, m/z, 532.53 (obsd. with 8 % abundance) (calcd.: m/z, 532.24) (Fig. S5 ESI†).

X-Ray crystallography

X-ray data of the suitable crystal of HL and complex **1** were collected on a Bruker's Apex-II CCD diffractometer using MoK_α (λ = 0.71073). The data were corrected for Lorentz and polarization effects and empirical absorption corrections were applied using SADABS from Bruker. The structures were solved by direct methods using SIR-92 and refined by full-matrix least squares refinement methods based on F^2, using SHELX-97.[9] All calculations were performed using Wingx package.[10] Important crystallographic parameters are given in Table S1 (ESI†). The crystallographic data of HL.NMe_2CHO and complex **1** have been deposited to Cambridge Crystallographic Data Centre bearing the CCDC nos. 953037 and 953036 respectively.

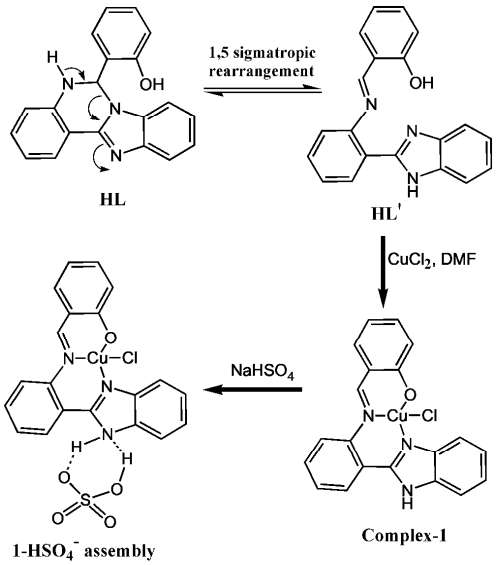

Scheme 1 Synthetic strategy of **1** and **1**-HSO_4^- assembly.

General method of absorption and fluorescence study

The pH study was done using 1 mM HEPES buffer solution by adjusting pH with HCl or NaOH. The stock solutions (~ 10^{-2} M) for the selectivity study of the probe **(1)** towards different anions were prepared taking sodium salt of perchlorate, cyanide, bi-carbonate, disodium hydrogen arsenate, tetra butyl ammonium salt of chloride, bromide, iodide, acetate, fluoride, hydrogen phosphate, dihydrogen phosphate and sodium hydrogen sulphate to the above solvent. In this selectivity study, the amounts of these anions were taken hundred times greater than that of the receptor. Fluorescence titration of **1** was performed with $NaHSO_4$. All the fluorescence and absorbance spectra were taken after 15 minutes of mixing of the components to acquire the optimized spectra. Fluorescence measurements were performed using 5 nm x 5 nm slit width.

Fluorescence quantum yields (Φ) were estimated by integrating the area under the fluorescence curves with the equation:

$$\phi_{sample} = \frac{OD_{standard} \times A_{sample}}{OD_{sample} \times A_{standard}} \times \phi_{standard}$$

where A is the area under the fluorescence spectral curve and OD is optical density of the compound at the excitation wavelength. The standard used for the measurement of fluorescence quantum yield was anthracene (Φ = 0.29 in ethanol). The binding constant values were determined from the

emission intensity data following the modified Benesi-Hildebrand equations[11,12]

$1/\Delta F=1/\Delta F_{max}+(1/K[C])(1/\Delta F_{max})$, $\Delta F=F_x-F_0$, $\Delta F_{max}=F_\infty-F$

where F_0, F_x, and F_{max} are the emission intensities of probe considered in the absence of any ion, at an intermediate concentration, and at a concentration of complete interaction, respectively, and where K is the binding constant and [C] is the concentration of the probe.

Job's plot from fluorescence experiments

A series of solutions containing complex **1** and $NaHSO_4$ were prepared such that the total concentration of complex **1** and $NaHSO_4$ remained constant (10 μM) in all the sets. The mole fraction (X) of $NaHSO_4$ was varied from 0.1 to 0.9. The fluorescence intensity at 480nm was plotted against the mole fraction of $NaHSO_4$.

Theoretical Calculation

To clarify the understanding of the ground state configurations of complex **1** and its corresponding **[1**.HSO_4**]**$^-$ adduct DFT calculations were performed using Gaussian-09 software over a Red Hat Linux IBM cluster. Molecular level interactions have also been studied using density functional theory (DFT) with the B3LYP/6-31G (d,p) functional model and basis set.[13] Vertical electronic excitations based on B3LYP optimized geometry was computed using the time-dependent density functional theory (TD-DFT)[14] formalism in water using conductor-like polarizable continuum model (CPCM)[15] to calculate the fractional contributions of various groups to each molecular orbital. The lowest 20 singlet states along the vertical excitation energies are computed here.

Redox studies

The electrochemical properties of complex **1** and **1** in presence of different ions have been studied by cyclic voltammetry (CV) on a Pt-wire as working electrode, a glassy carbon as a counter electrode, and an Ag/AgCl as reference electrode in DMF solution (0.1 M TBAP as supporting electrolyte) at room temperature.

In *vitro* cell imaging

Human cervical cancer cell, HeLa cell line was purchased from National Center for Cell Science (NCCS), Pune, India and was used throughout the study. Cell were cultured in Dulbecco's modified Eagle's medium (DMEM, Gibco BRL) supplemented with 10% fetal bovine serum (FBS) (Gibco BRL), and 1% antibiotic mixture containing penicillin, streptomycin and neomycin (PSN, Gibco BRL), at 37 °C in a humidified incubator with 5% CO_2. For experimental study, cells were grown to 80-90 % confluence, harvested with 0.025 % trypsin (Gibco BRL) and 0.52 mM EDTA (Gibco BRL) in phosphate-buffered saline (PBS, Sigma Diagnostics) and plated at desire cell concentration and allowed to re-equilibrate for 24h before any treatment. Cells were rinsed with PBS and incubated with DMEM-containing **1** (10 μM, 1% DMSO) for 30 min at 37 °C. All experiments were conducted in DMEM containing 10% fetal bovine serum (FBS) and 1% PSN antibiotic. The imaging system was composed of a fluorescence microscope (ZEISS Axioskop 2 plus) with an objective lens [10×].

Cell Cytotoxicity Assay

To test the cytotoxicity of complex **1**, MTT [3-(4,5-dimethyl-thiazol-2-yl)-2,S-diphenyl tetrazolium bromide] assay was performed by the procedure described earlier.[16] After treatments of the probe (5, 10, 20, 50, and 100 μM), 10μl of MTT solution (10 mg/ml phosphate-buffered saline) was added in each well of a 96-well culture plate and incubated continuously at 37°C for 12 h. All mediums were removed from wells and replaced with 100μl of acidic isopropanol. The intracellular formazan crystals (blue-violet) formed were solubilized with 0.04 N acidic isopropanol and the absorbance of the solution was measured at 595 nm wavelength with a microplate reader. Data are given as the mean ± S.D. of three independent experiments. The cell cytotoxicity was calculated based on a cell viability of 100%.

Results and discussion

Synthesis and structural characterisation

Organic moiety HL was synthesized by simple facile condensation of *2-(2-aminophenyl) benzimidazole* with *2-hydroxy-benzaldehyde* in MeOH. Complex **1** was prepared by the complexation reaction of HL with $CuCl_2$ in DMF-methanol mixed solvent. The structures of HL and complex **1** were characterized by physico-chemical and spectroscopic tools along with the detailed structural analyses by single crystal X-ray diffraction (Fig. 1). Complex **1** was formed through 1,5-σ tropic shift[8,17] to generate *2-{[2-(1H-benzoimidazol-2-yl)-phenyl-imino]-methyl}-phenol* (HL′) leaving a free N-H for which the solubility of complex **1** in water is much more than that of HL (Scheme 1).

The solid **1**-HSO_4^- ensembled species was obtained from the reaction of *sodium hydrogen sulphate* with methanolic solution of [Cu(L′)(Cl)] in 1:1 mole ratio at stirring condition. The ESI mass spectrum of **1**-HSO_4^- in methanol shows a molecular-ion peak at m/z 532.53 with ~8% abundance, which can be assigned to $[M+H]^+$ (calculated value at m/z, 532.40). A characteristic peak for $\nu_{S=O}$ at 1184 cm^{-1} in the FTIR spectrum of [Cu(L′)(Cl)] confirms the existence of sulphate ion.[18]

Single crystals of the organic moiety (HL) and the probe, **1** were obtained as HL.NMe_2CHO and [Cu(L′)(Cl)] respectively from the DMF-MeOH mixed solution. The HL.NMe_2CHO crystallizes in the monoclinic space group Cc and [Cu(L′)(Cl)] crystallizes in the triclinic space group P-1. ORTEP view of the complex **1** and probe (HL) with atom labelling scheme are illustrated in Fig. 1 and Fig. S6†. The selected bond distances and bond angles are listed in Table S2 and S3 (ESI†) respectively.

The bond C20-O1 (1.356(5) Å) in HL is somewhat longer than the corresponding bond, C16-O1 (1.311(3) Å) in complex **1** due

to the complexation. The occurrence of 1,5-sigmatropic shift (Scheme 1) helps the rearranged form of HL to act as tridentate monobasic ligand to form the four coordinated complex **1** which is distorted square planar copper(II) complex coordinating with phenolate-O, imine-N and imidazolic-N of the rearranged form of HL and chloride ion. Here, the bond distance of C7-N2 (1.354(4) Å) in HL is reduced to 1.336(3) Å (C7-N3) in the complex-**1**, Hydrogen bonds along with some other weaker interactions are responsible for the crystal packing to form a 1D chain and a 2D layered arrangement (Fig. S7 ESI†).

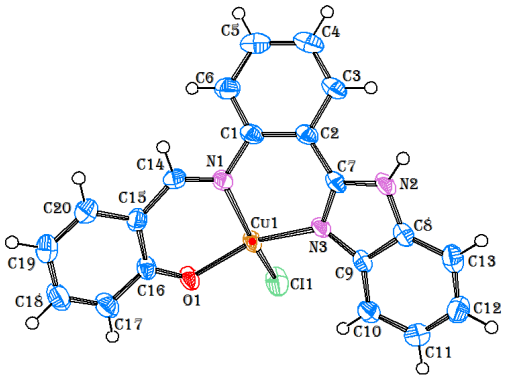

Fig. 1 An ORTEP view (50% probablity) with atom numbering scheme of complex **1**.

UV-vis spectroscopic studies

Addition of $NaHSO_4$ to the solution of **1**, green color changed to light green color depicted in Fig. 2 due to the formation of 1-HSO_4^- ensembled species in water : DMSO (9 : 1, v/v) at biological pH (using 1 mM HEPES buffer). Here, the characteristic d-d band for copper(II) complex centered at *ca.* 403 nm was gradually decreased along with the band at *ca.* 293 nm.

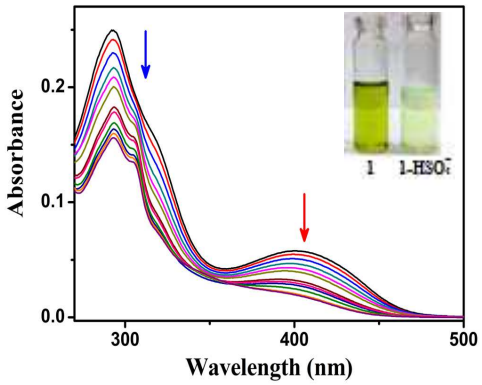

Fig. 2 UV-vis titration spectra of complex **1** (10 μM) upon incremental addition of HSO_4^- ions (0-20 μM) in water : DMSO (9 : 1, v/v) at 25 ^oC, Inset: naked eye colour change of complex 1 followed by addition of $NaHSO_4$.

Fluorescence spectroscopic studies

HL has blue fluorescence with an emission peak *ca.* at 430 nm. Addition of HSO_4^- ions to the solution of HL results in quenching of the fluorescence due to the assistance of reductive PET process towards fluorophore benzimidazole unit (*vide* Scheme S2). As a result, gradual addition of HSO_4^- ions led to a systematic decrease in the fluorescence ntensity (Fig. S8 ESI†). This process has been hindered by blocking the phenolic-OH through complex formation. For this purpose we performed the selectivity study with different metal ions (Fig. S9 ESI†) and we found that HL is highly selective and specific toward Cu^{2+} ions and get a systematic decrease in the fluorescence intensity with the gradual increase of the Cu^{2+} ions concentration resulting in a complete quenching of fluorescence intensity through complex formation (complex **1**) (Fig. S10 ESI†). Complex **1** was formed *via* 1,5-sigmatropic shift resulting in a free imidazolic N-H which helps to welcome the HSO_4^- ions to form the six membered cyclic ring adduct $[1.HSO_4]^-$ through intermolecular H-bonding (*vide* Scheme 2, S2†). On addition of HSO_4^- ions to the solution of **1**, an emission band appeared at *ca.* 480 nm when excited at λ_{ex}= 390 nm and was gradually enhanced with the increasing concentration of HSO_4^- ions (Fig. 3) with a high quantum yield (Φ_f = 0.51) (*vide* Table 1).

Emission intensity of the off-on system at various pH recorded in HEPES buffer. In presence of HSO_4^- ions lower intensity was observed below pH 6.0 and showed pH independency over the pH range ~6.0 to 8.0 i.e. in the biological pH range (Fig. S11 ESI†). This variable pH test suggests that the probe is reliable, selective, and biocompatible fluorescence probe for HSO_4^- in the biological pH reasonably. This pH region for sensing HSO_4^- also makes it very useful application in detection in waste water, industrial trade analysis and physiological treatment.

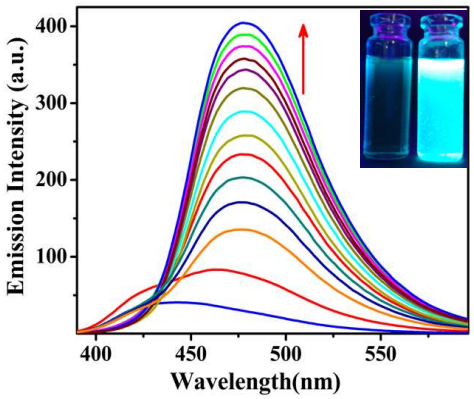

Fig. 3 Emission spectra of complex **1** (10 μM) upon incremental addition of HSO_4^- ions (0-20 μM), Inset: fluorescence colour change of complex **1** with the addition of $NaHSO_4$ (λ_{ex}= 390 nm).

To investigate compatibility of the ensemble-based anion detection ability of **1**, emission spectra of complex **1** in water : DMSO (9 : 1, v/v) were examined with respect to various anions. Indeed, as shown in Fig. S12 in the SI, complex **1** revealed remarkable enhancement of emission intensity only in the presence of HSO_4^- ions, whereas no noticeable changes were observed with other anions F^-, Cl^-, Br^-, I^-, CN^-, AcO^-, HCO_3^-, HPO_4^{2-}, $H_2PO_4^-$, SO_4^{2-}, NO_3^-, ClO_4^-, N_3^- and $H_2AsO_4^-$. This competitive experiment shows high selectivity of complex **1** towards HSO_4^- ions. On gradual addition of HSO_4^- ions to the

aqueous solution of complex **1**, emission intensity at 480 nm simultaneously increases. No significant interference was observed when different anion salts were added in **1**.HSO_4^- assembled mixture (Fig. S13 ESI†). Job's plot analysis from the fluorescence titration spectra exhibited a maximum at 0.5 mol fractions of HSO_4^- ions, indicating formation of a 1:1 complex between complex **1** and HSO_4^- ions (Fig. S14 ESI†). On the basis of the 1:1 stoichiometry and fluorescence titration data from Fig. 3, the association constant (K_a) of complex **1** for HSO_4^- was calculated to be 1.4×10^5 M^{-1} (Fig. S15 ESI†) which indicate a stronger binding affinity towards the HSO_4^- ions. The detection limit in this process was significantly low to be 3.18×10^{-7} M HSO_4^- ions in water : DMSO (9 : 1, v/v) (Fig. S16 ESI†). The linearity of this experimental method of detection of HSO_4^- ions was verified (*vide* Fig. S17 ESI†) and it was found to be 3.18 x 10^{-7} to 1.25 x 10^{-5} mol L^{-1} of HSO_4^- ions within a very short responsive time (5-10 s).

The fluorescence average life time (τ) of the complex **1** in water: DMSO (9 : 1, v/v) was determined by time resolved spectrum (Fig. 4) and it was found to be 7.64 ns. After gradual addition of $NaHSO_4$ the value of B_2 increases and B_1 decreases indicating strong interactions with complex **1**. According to the equations: $\tau^{-1} = k_r + k_{nr}$ and $k_r = \Phi_f/\tau$,[19] the radiative rate constant, k_r and total nonradiative rate constant k_{nr} of **1**-HSO_4^- assembly are given in (Table 1). The data suggest that the factor which induce fluorescent enhancement is mainly ascribed to the gradual increase of k_r and decrease of k_{nr}.

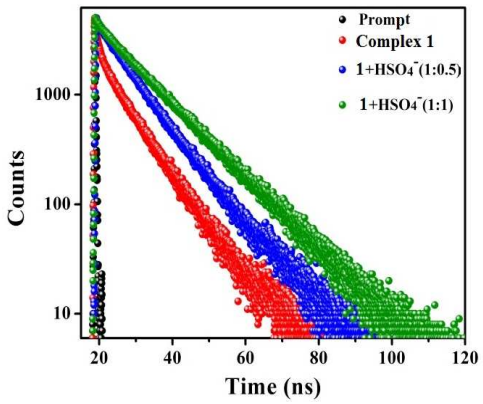

Fig. 4 Time-resolved fluorescence decay of complex **1** and **1**-HSO_4^- system (0.5 equivalent and 1.0 equivalent) in water : DMSO (9 : 1, v/v) at 25 °C using a nano LED of 377 nm as the light source at λ_{em} = 480 nm.

Table 1 Fluorescence quantum yield (Φ_f) and life time (τ_f in ns) of the corresponding singlet excited states at λ_{em} = 480 nm.

	B_1	B_2	τ_{av} (ns)	χ^2	φ	k_r (10^8 s^{-1})	k_{nr} (10^9 s^{-1})
Complex **1**	13.8	86.5	7.64	1.067	0.07	0.092	0.122
1 + HSO_4^- (1 : 0.5)	11.96	88.04	10.08	1.073	-	-	-
1 + HSO_4^- (1 : 1)	4.18	95.82	12.44	1.068	0.51	0.409	0.039

Electrochemical study

To insight this fact of the sensing pathway, the electrochemical study of the isolated complex **1** in absence and, in presence of HSO_4^- ions and some closely competitive anions was carried out using *tetrabutylammonium perchlorate* (TBAP) as supporting electrolyte in DMF (*vide* Fig. 5, and Figs. S18 and S19 ESI†). Cyclic voltammograms depicted in Fig. 5 indicates that the Cu^{2+}/Cu^+ redox couple of complex **1** in presence of HSO_4^- ions appeared at less cathodic (*ca.* -0.29 V (*vs*. Ag/AgCl)) compared to that of complex **1** in absence of HSO_4^- ions (*ca.* -0.38 V (*vs*. Ag/AgCl)). The electron-deficient nature of the Cu^{2+} ion in [**1**.HSO_4]$^-$ adduct is clearly evident in the potentials difference, which were shifted by 90 mV toward less negative compared to that of Cu^{2+} ion in complex **1**, pointing out the easy reduction of Cu^{2+}-benzimidazole unit in [**1**.HSO_4]$^-$ adduct. This significant shift in the reduction potentials supports the strong electron-withdrawing effect of the HSO_4^- ion in ring form present in [**1**.HSO_4]$^-$ adduct.

To strengthen the fact of binding of HSO_4^- ions with the pyrolic-N through hydrogen bonding, the electrochemical behavior of complex **1** was verified in presence of HCl and HCl *plus* SO_4^{2-} ions (*viz.* Fig. S18 ESI†). Here, the Cu^{2+}/Cu^+ redox couple of complex **1** duly protonated by HCl was significantly shifted to anodically to *ca.* -0.23 V (*vs*. Ag/AgCl) (*vide* Table S4), but in case of the addition of SO_4^{2-} ions after HCl, the Cu^{2+}/Cu^+ redox couple was observed at *ca.* -0.28 V (*vs*. Ag/AgCl) which is very close to the observed potential for this couple in presence of HSO_4^- ions (*ca.* -0.29 V *vs*. Ag/AgCl).

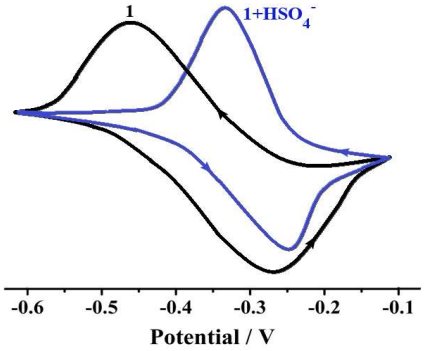

Fig. 5 Cyclic voltammogram (scan rate 100 mV/s) of complex **1** and **1**.HSO_4^- adduct in DMF solution containing 0.1 M TBAP, using platinum working electrode.

The binding of HSO_4^- ion with the pyrrolic-N of **1** through hydrogen bonding is also in support of the DFT calculation and p-MO electron distribution which showed that the energy of LUMO (--2.3082 eV) in [**1**.HSO_4]$^-$ adduct is less than that of LUMO (-2.0881 eV) in complex **1**. And this is also reflected in the reduction of the bond length of Cu1-N3 (theoretically calcd. 1.8739 Å) in [1.HSO_4]$^-$ adduct from that of Cu1-N3 (obsd. 1.9591(18) Å or calcd. 1.9589 Å both) in complex **1** by significant value.

ESR Spectra

ESR spectrum of the complex **1** at liquid nitrogen temperature (120 K) in MeOH showed four well resolved peaks in the low field region (Fig. S20 ESI†) corresponding to $g_\parallel$ (2.259) and $g_\perp$

(2.019). The trend $g_{\parallel}$ (2.259) > $g_{\perp}$ (2.019) > g_e (2.0023) observed for the copper complex suggests that the unpaired electron is localized in the d_{x2-y2} orbital of the copper ion.[20] The fact that the unpaired electron lies predominately in the d_{x2-y2} orbital is also supported by the value of the exchange interaction term G estimated from expression:

$$G = (g_{\parallel} - 2.0023) / (g_{\perp} - 2.0023)$$

If $G > 4.0$, the local axes are aligned parallel or only slightly misaligned. If $G < 4.0$, significant exchange coupling is present and the misalignment is appreciable. The observed value for the exchange interaction parameter for the Cu(II) complex (G = 15.37) suggests that the local tetragonal axes are aligned parallel or slightly misaligned and that the unpaired electron is present in the d_{x2-y2} orbital.

ESR spectrum of the **[1.HSO$_4$]$^-$** adduct (Fig. 6) at liquid nitrogen temperature also showed four well resolved peaks in the low field region corresponding to $g_{\parallel}$ (2.265) and $g_{\perp}$ (2.026) conforming the same square planer geometry by putting the unpaired electron in the d_{x2-y2} orbital (G = 11.08).

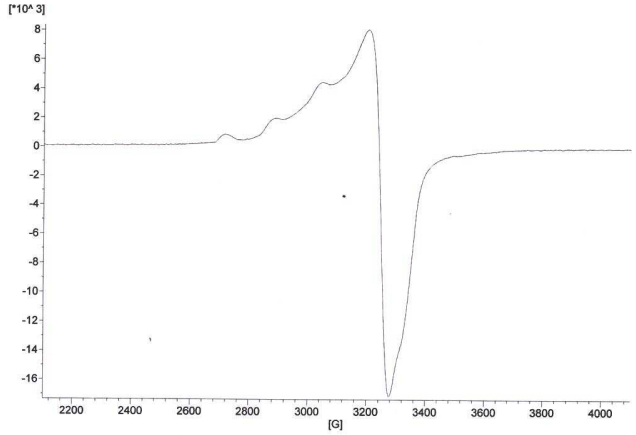

Fig. 6 EPR spectrum of the **[1.HSO$_4$]$^-$** adduct in methanol at 120 K.

Geometry optimization

The interaction pattern of complex **1** with HSO_4^- was confirmed by theoretical DFT calculations. The HSO_4^- ions interacts with complex **1** by forming intermolecular H-bonding. It was interesting to note that, the 1:1 stoichiometry may be possible by linear interaction (A path) or by ring formation (B path) (Fig. 7). But energy gap between HOMO and LUMO in the B path is lower (2.4383 eV) than that of path A (2.8923eV) (Table S5-S6 ESI†). So, chelate ring formed structure is more stabilized and conjugated (i.e.; extension of π conjugation) than linear structure. Such introduced of the ring system may reduce the paramagnetic effect of Cu^{2+} in complex **1** which was further cleared by investigation of the contours of the electronic distribution. The p-MO surfaces of the electronic distribution in highest occupied molecular orbital (HOMO) and lowest unoccupied molecular orbital (LUMO) states on these molecules suggested that there were very essential differences between compounds [**1**.HSO$_4$]$^-$ and complex **1** (Fig. 7). Precisely, the HOMO and LUMO states of the complex **1** resided over the salicylaldehyde moiety. Addition of HSO_4^- ions in complex **1** shifted the HOMO from Cu^{2+} ion to HSO_4^- ring. This restoring of electron density was more promising in the ring system over chain. The electron withdrawing ability of the [**1**.HSO$_4$]$^-$ in ring system give a clear idea that the Cu^{2+} ion in [**1**.HSO$_4$]$^-$ adduct are easily reducible, which is in agreement with our experimental results getting from cyclic voltammetry.

The UV spectra computed from TDDFT calculations in water show two important peaks in the range of 310-450 nm. For complex 1, the band around 397.43 nm is dominated by the HOMO → LUMO; HOMO → LUMO+1 excitation, while the band around 313.01 nm is mainly due to HOMO-4 → LUMO+1; HOMO-1 → LUMO+1 transitions (Fig. S21 ESI†). The details of the vertical excitation energies, oscillator strengths, and salient transitions are shown in Table S7 in the SI. For **1**.HSO_4^- adduct the band around 410.25 nm is dominated by the HOMO-1 → LUMO; HOMO-2 → LUMO; HOMO-3 → LUMO transitions while the band around 321.58 nm is mainly due to HOMO → LUMO+2; HOMO → LUMO+3; HOMO → LUMO+4 transitions (Fig. S22 ESI†) as tabulated in Table S8 (ESI†). Here, the calculated spectra of the complexes are found to be in well match with the experimental ones.

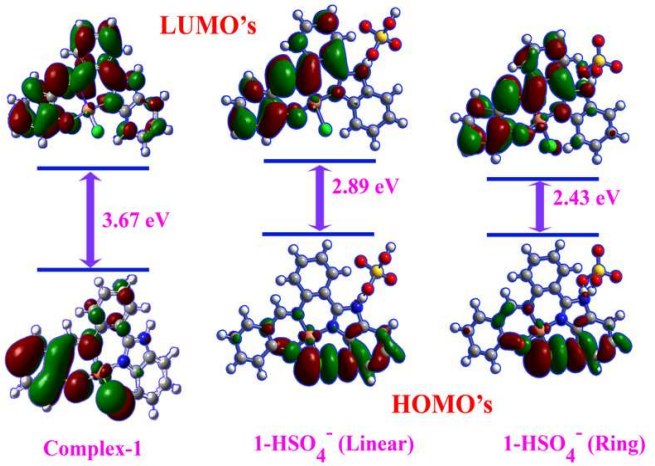

Fig. 7 Molecular orbital (MO) diagram of complex **1** with energy difference and for the interactions of HSO_4^- ions with complex **1** by linear interaction (path A) or by ring formation (path B).

Probable Mechanism

On the basis of the above observation in fluorescence spectroscopic studies, the probable mechanism could be stated as follows. If the enhancement of the fluorescence would be related with the phenomena of coordination of HSO_4^- ions to the copper(II) then fluoride/cyanide ions which are of more coordinating nature than that of weak HSO_4^- ions, could interfere the selectivity of the probe towards HSO_4^- ions. Spectroscopic study is against the removal of Cu(II) centre by HSO_4^- ions. Again, the ligation of imidazolic-N with copper(II) ion through chelation helps the other pyrrolic-N to bind HSO_4^- ions through hydrogen bonding in support of the selective enhancement of fluorescence of the system in '*turn-on*'

style based on intermolecular hydrogen bonding assisted chelation enhanced fluorescence (CHEF) process; and this is similar with the previous report in which the attachment of the proton to the imidazolic-N of the organic moiety facilitate the recognition of HSO_4^- ions by ring formation through hydrogen bonding with pyrrolic-N atom.[7c,l]

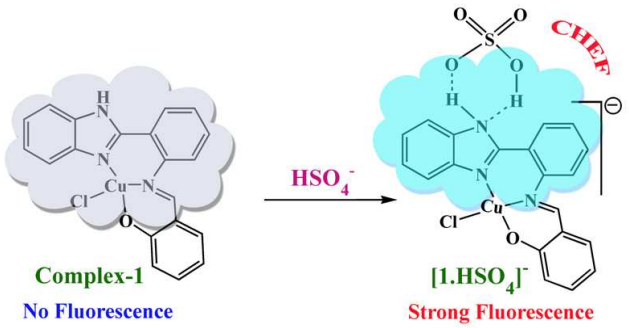

Scheme 2 Plausible mechanism of hydrogen sulphate sensing.

The formation of complex **1** was possible *via* 1,5-sigmatropic shift in HL leaving the pyrolic-N to welcome the HSO_4^- ions to form the adduct $[\mathbf{1}.HSO_4]^-$ (*vide* Scheme 2). Added HSO_4^- ions bonded with the pyrolic-N through intermolecular H-bonding by forming stable six membered chelate ring (*viz*. theoretical calculation), which has pulled the electron density from the metal centre Cu^{2+} ion and this fact is in support of the enhancement of the fluorescence through chelation.

The electron density over N1, N2, O1, H1 etc (*viz*. Fig. S23 ESI†) these atoms in **HL** were partially pulled when the organic moiety (**HL′**) binds with Cu(II) ions which was in favor of paramagnetic effect (quenching) of Cu(II) ions. But addition of HSO_4^- ions to the complex-**1** enhancement of the fluorescence intensity (CHEF) by partial back pulling of electron density towards the benzimidazole unit. This fact was established by NPA calculation (Fig. S23 ESI†), where the NPA charge density over the above mentioned atoms was first dragged due to chelation with Cu(II) ions and it was again partially recovered when HSO_4^- ions was added to the solution of complex-**1**.

Biological studies

To examine the utility of the probe in biological systems, it was applied to human cervical cancer HeLa cell. In this experiment complex **1** was allowed to uptake by the cells of interest and the images of the cells were recorded by the fluorescence microscopy following excitation at ~390 nm. After incubation with complex **1** (10 μM) for 30 min the cell displayed very faint intracellular fluorescence image due to the very weak emission *ca*. at 430nm. However, cells exhibited intensive fluorescence when exogenous HSO_4^- ions were introduced into the cell via incubation with $NaHSO_4$ in the previously preloaded complex **1** cells (Fig. 8).

Fluorescence intensity increases due to significant interactions of complex **1** with HSO_4^- ion at biological pH. In addition, the *in vitro* study showed that 10 μM of complex **1** did not show any cytotoxic effect to cell upto 6 h (Fig. S24 ESI†). These results indicate that the probe, **1** has a huge potentiality for both *in vitro* and *in vivo* application as well as imaging in different ways as same manner for live cell imaging.

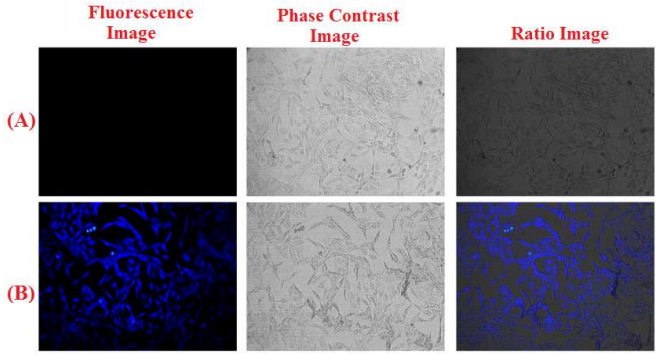

Fig. 8 Fluorescence image of HeLa cells encumbered with (A) complex **1** (10.0 μM); (B) Complex **1** (10.0 μM) with 10.0 μM HSO_4^- solution. All the samples were excited at 390 nm with emission 480 nm by using a [10X] objective.

Conclusion

In summary, a water soluble copper(II) complex (**1**) has been developed as a HSO_4^- ion selective chemosensor in '*turn-on*' style based on intermolecular hydrogen bonding assisted chelation enhanced fluorescence (CHEF) process in water : DMSO (9 : 1, v/v). To establish the proposed 'off-on' mechanism for selective sensing of the HSO_4^- ions, thorough experimental and theoretical studies have been carried out systematically. Interestingly, the competitive anionic species do not affect the detection of HSO_4^- ions and it is also useful for bioimaging of the intracellular HSO_4^- ions. Herein, HSO_4^- ion neither coordinate with Cu^{2+} centre nor replace the Cu^{2+} ion to be a HSO_4^- ions selective chemosensor but it happens through intermolecular hydrogen bonding to form the six membered cyclic ring adduct $[\mathbf{1}.HSO_4]^-$, which has been ascertained by electrochemical and spectroscopic including theoretical studies.

Acknowledgements

Financial assistance from CSIR, New Delhi, India is gratefully acknowledged. B. Sen wishes to thank to UGC, New Delhi, India for offering him the fellowship. The authors are grateful to USIC, The University of Burdwan for the single crystal X-ray diffractometer facility under PURSE program. We sincerely acknowledge Mr. Samya Banerjee, IPC department, IISC, Bangalore for acquiring the cell images using fluorescence microscope.

Notes and references

[a] Department of Chemistry, Burdwan University, Golapbag, Burdwan-71 3104, West Bengal, India. E-mail: pabitracc@yahoo.com

†Electronic Supplementary Information (ESI) available: [Tables, schemes, figures, characterization data, and some spectral data] and CIF

of HL.NMe$_2$CHO and complex **1** are available free of charge *via* the internet at http://pubs.rsc.org. See *DOI: 10.1039/x0xx00000x.*

‡CCDC no's for HL.NMe$_2$CHO and complex **1** are **953037** and **953036** respectively.

Corresponding Author

* E-mail: pabitracc@yahoo.com. Tel: +91-342-2558554 extn. 424. Fax: +91-342-2530452.

References

1. (a) T. Y. Joo, N. Singh, G. W. Lee, D. O. Jiang, *Tetrahedron Lett.*, 2007, **48**, 8846; (b) J. M. Hermida-Ramon, C. M. Estevez, *Chem. Eur. J.*, 2007, **13**, 4743; (c) P. A. Gale, *Acc. Chem. Res.* 2006, **39**, 465; (d) E. A. Katayev, Y. A. Ustynyuk, J. L. Sesser, *Coord. Chem. Rev.*, 2006, **250**, 3004; (e) F. P. Schmidtchen, *Coord. Chem. Rev.*, 2006, **250**, 2918; (f) V. Amendola, M. Bonizzoni, D. Esteban-G´omez, L. Fabbrizzi, M. Licchelli, F. Sancenon, A. Taglietti, *Coord. Chem. Rev.*, 2006, **250**, 1451.
2. (a) I. Ravikumar P. Ghosh, *Chem. Soc. Rev.*, 2012, **41**, 3077; (b) M.E. Moragues, R. Martinez-Manez, F. Sancenon, *Chem. Soc. Rev.*, 2011, **40**, 2593; (c) A. F. Li, J. H. Wang, F. Wang, Y. B. Jiang, *Chem. Soc. Rev*., 2010, **39**, 3729; (d) R. M. Duke, E. B. Veale, F. M. Pfeffer, P. E. Kruger, T. Gunnlaugsson, *Chem. Soc. Rev*., 2010, **39**, 3936; (e) P. A. Gale, *Chem. Soc. Rev.*, 2010, **39**, 3746; (f) C. Bazzicalupi, A. Bencini, S. Biagini, E. Faggi, S. Meini, C. Giorgi, A. Spepi, B. Valtancoli, *J. Org. Chem*., 2009, **74**, 7349; (g) E.J.O. Neil, B.D. Smith, *Coord. Chem. Rev.*, 2006, **250**, 3068.
3. J. W. Pflugrath and F. A. Quiocho, *Nature*, 1985, **314**, 257.
4. B. A. Moyer, L. H. Delmau, C. J. Fowler, A. Ruas, D. A. Bostick, J. L. Sessler, E. Katayev, G. D. Pantos, J. M. Linares, Md. A. Hossain, S. O. Kang, K. Bowman-James, *In Advances in Inorganic Chemistry: Template Effects and Molecular Organisation*, **59**.
5. P. I. Jalava, R. O. Salonen, A. S. Pennanen, M. S. Happo, P. Penttinen, A.I. Healinen, M. Sillanpae, R. Hillamo and M. R. Hirvone, *Toxicol. Appl. Pharmacol*., 2008, **229**, 146.
6. F. P. Schmidtchen, *Top. Curr. Chem.*,1986, **132**, 101.
7. (a) R. Shen, X. B. Pan, H. F. Wang, L. H. Yao, J. C. Wu and N. Tang, *Dalton Trans.*, 2008, 3574; (b) H. J. Kim, S. Bhuniya, R. K. Mahajan, R. Puri, H. G. Liu, K. C. Ko, J. Y. Lee and J. S. Kim, *Chem. Commun.*, 2009, 7128; (c) M. Alfonso, A. Tarraga, P. Molina, Org. Let., 2011, **13**, 6432; (d) A. Mallick, T. Katayama, Y. Ishibasi, M. Yasudab and H. Miyasaka, *Analyst*, 2011, **136**, 275; (e) V. Kumar, A. Kumar, U. Diwan, K. K. Upadhyay, *Chem. Commun.*, 2012, **48**, 9540; (f) S. T. Yang, D. J. Liao, S. J. Chen, C. H. Hu and A. T. Wu, *Analyst*, 2012, **137**, 1553; (g) J. Chang, Y. Lu, S. He, C. Liu, L. Zhao and X. Zeng, *Chem. Commun.*, 2013, **49**, 6259; (h) W. Lu, J. Zhou, K. Liu, D. Chen, L. Jiang, Z. Shen, *J. Mater. Chem. B*, 2013, **1**, 5014; (i) L. Wang, L. Yang, D. Cao, *J. Fluoresc*, 2014, **24**, 1347; (j) D. Sarkar, A. K. Pramanik, T. K. Mondal, *RSC Adv.*, 2014, **4**, 25341; (k) M. Mukherjee, S. Pal, B. Sen, S. Lohar S. Banerjee, S. Banerjee, P. Chattopadhyay, *RSC Adv*., 2014, **4**, 27665; (l) M. Mukherjee, B. Sen, S. Pal, S. Banerjee, S. Lohar, E. Zangrando, P. Chattopadhyay, *RSC Adv*., 2015, **5**, 4468; (m) B. Sen, M. Mukherjee, S. Pal, S. K. Mondal, M. S. Hundal, A. R. Khuda-Bukhsh, P. Chattopadhyay, *RSC Adv.*, 2014, **4**, 15356 and references therein.
8. W. Cao, X. J. Zheng, D. C. Fang and L. P. Jin, *Dalton Trans*., 2015, **44**, 5191.
9. G. M. Sheldrick, Shelxs97 and shelxl97 programs for crystallography University of Göttingen: Germany, 1997.
10. (a) X. Zhou, P. Li, Z. Shi, X. Tang, C. Chen and W. Liu, *Inorg Chem.*, 2012, **51**, 9226; (b) A. Altomare, G. Cascarano, C. Giacovazzo and A. Guagliardi, *J. Appl. Crystallogr*., 1993, **26**, 343; (c) G. M. Sheldrick, *Acta Cryst A*, 2008, **64**, 112; (d) L. J. Farrugia, *J. Appl. Cryst.*, 1999, **32**, 837.
11. A. Mallick, N. Chattopadhyay, *Photochem. Photobiol*., 2005, **81**, 419.
12. H. A. Benesi, J. H. Hildebrand, *J. Am. Chem. Soc.*, 1949, **71**, 2703.
13. (a) M. Cossi, N. Rega, G. Scalmani, V. Barone, *J. Comput. Chem.*, 2003, **24**, 669; (b) M. Cossi, V. Barone, *J. Chem. Phys.*, 2001, **115**, 4708; (c) V. Barone, M. Cossi, *J. Phys. Chem. A*, 1998, **102**, 1995.
14. M. E. Casida, C. Jamorski, K. C. Casida, D. R. Salahub. *J. Chem. Phys.*, 1998, **108**, 4439.
15. N. M. O' Boyle, A. L. Tenderholt, K. M. Langner, *J. Comput. Chem.*, 2008, **29**, 839.
16. J. Ratha, K. A. Majumdar, S. K. Mandal, R. Bera, C. Sarkar, B. Saha, C. Mandal, K. D. Saha, R. Bhadra, *Mol. Cell Biochem*., 2006, **290**, 113.
17. (a) S. Pal, M. Mukherjee, B. Sen, S. Lohar P. Chattopadhyay, *RSC Adv.*, 2014, **4**, 21608; (b) M. Mukherjee, B. Sen, S. Pal, M.S. Hundal, S. K. Mandal, A. R. Khuda-Bukhsh and P. Chattopadhyay, *RSC Adv*., 2013, **3**, 19978; (c) S. Sen, S. Sarkar, B. Chattopadhyay, A. Moirangthem, A. Basu, K. Dhara and P. Chattopadhyay, *Analyst*, 2012, **137**, 3335; (d) H. Paul, T. Mukherjee, M. G. B. Drew and *P. Chattopadhyay*, *J. Coord. Chem.*, 2012, **65**, 1289; (e) U. C. Saha, B. Chattopadhyay, K. Dhara, S. K. Mandal, S. Sarkar, A. R. Khuda-Bukhsh, M. Mukherjee, M. Helliwell and *P. Chattopadhyay*, *Inorg. Chem.*, 2011, **50**, 1213.
18. J. Zhou, D. T. Moore, L. Wöste, G. Meijer, D. M. Neumark, K. R. Asmis, *J. Chem. Phys.*, 2006, **125**, 111102.
19. N. J. Turro, Modern Molecular Photochemistry; Benjamin/ Cummings Publishing Co., Inc.: Menlo Park, CA, 1978.
20. (a) B. J. Hathaway, A. A. G. Tomlinson, *Coord. Chem. Rev.*, 1970, **5**, 1; (b) R. Bakshi, M. Rossi, F. Caruso, P. Mathur, Inorg. Chim. Acta, 2011, **376**, 175.

